Drift-wave stability in the field-reversed configuration

C. K. Lau,[1,a)] D. P. Fulton,[2] I. Holod,[1] Z. Lin,[1,b)] M. Binderbauer,[2] T. Tajima,[1,2] and L. Schmitz[3]
[1]*University of California, Irvine, California 92697, USA*
[2]*Tri Alpha Energy, Inc., Rancho Santa Margarita, California 92688, USA*
[3]*University of California, Los Angeles, California 90095, USA*

(Received 10 May 2017; accepted 29 June 2017; published online 2 August 2017)

Gyrokinetic simulations of C-2-like field-reversed configuration (FRC) find that electrostatic drift-waves are locally stable in the core. The stabilization mechanisms include finite Larmor radius effects, magnetic well (negative grad-B), and fast electron short circuit effects. In the scrape-off layer (SOL), collisionless electrostatic drift-waves in the ion-to-electron-scale are destabilized by electron temperature gradients due to the resonance with locally barely trapped electrons. Collisions can suppress this instability, but a collisional drift-wave instability still exists at realistic pressure gradients. Simulation results are in qualitative agreement with C-2 FRC experiments. In particular, the lack of ion-scale instability in the core is not inconsistent with experimental measurements of a fluctuation spectrum showing a depression at ion-scales. The pressure gradient thresholds for the SOL instability from simulations are also consistent with the critical gradient behavior observed in experiments. *Published by AIP Publishing.* [http://dx.doi.org/10.1063/1.4993630]

I. INTRODUCTION

A field-reversed configuration (FRC) is an elongated prolate compact toroid (CT) with purely poloidal magnetic fields. The FRC consists of two regions separated by a separatrix: an inner, closed field-line core region and an outer, open field-line scrape-off layer (SOL) region. Research interest in the FRC persists because of potential reactor benefits: (1) the FRC is a plasma with β (the ratio of plasma pressure to magnetic energy density) near unity, which suggests less magnetic energy investment and less cyclotron radiation than low β approaches such as the tokamak; (2) the compact nature of the plasma simplifies the construction of the device hull and external magnetic field coils; (3) engineering is also aided by the SOL, which naturally connects to the divertor; and (4) the lack of toroidal magnetic fields radically changes the magnetic topology and the consequential stability of the plasma, as detailed below.

It was suggested by Rostoker *et al.*[1,2] that adding a significant energetic ion population via neutral beam injection (NBI) would improve FRC macro-stability while preserving the FRC's favorable transport properties[1,3–7] due to the large ion Larmor radius relative to the plasma size.[5,8] In 2008, Tri Alpha Energy, Inc. (TAE), launched a campaign on the FRC experiment, C-2.[9] With the use of NBI, electron gun biasing, and magnetic end plugs, the C-2 experiments have succeeded in suppressing the major MHD instabilities, the rotational ($n = 2$), wobble, and tilt[10] ($n = 1$) modes (where n is the toroidal mode number), and increasing FRC confinement times to the order of several milliseconds.[10–12] This achievement has made the FRC reach the transport-limited regime.

In early experiments of FRCs, besides the fact that many FRCs may not have reached the transport-limited regime, the transport studies have showed relatively short confinement times. In these experiments, particle,[13,14] flux,[15] and energy confinement were well identified as anomalous. Possible electrostatic micro-instabilities have been investigated,[16–19] with the lower hybrid drift instability (LHDI) theoretically identified as the most linearly unstable. However, experiments found that the LHDI saturates at levels two orders of magnitude below oft-predicted values.[16] Electromagnetic modes such as the electron temperature gradient driven electromagnetic micro-tearing modes may also be present in FRCs[20] but have not been studied in detail. Confinement is significantly affected by radial diffusion through the edge,[21,22] where particles move from the closed field-lines of the core to the open field-lines of the SOL. A number of analytical studies have been made of classical transport in simple equilibria[23–26] and using quasi-steady 1-D plasma profiles.[27–29] Numerical models of transport have been made to include more details using both simple 1-D and 2-D equilibria.[13,15,30–33]

However, once the FRC plasmas in C-2 and C-2U[10–12,34] clearly reached the transport-limited regime with sufficient remedies of macro-instabilities mentioned earlier, the transport times have been found to lengthen considerably[12] and show markedly different properties of fluctuations.[35] In these FRC shots, the Q1D fluid transport code,[36] based on the CFRX code,[37] has been developed and employed for transport analysis of C-2 plasma conditions.

Schmitz *et al.*[35] found that, while the plasma in the SOL shows robust fluctuations driven by micro-instabilities, the level of fluctuations in the FRC core is less than in the SOL by 1–2 orders of magnitude. The level of fluctuations is reduced when the neutral beam injection commences. An appropriately applied end voltage bias can further reduce the level of fluctuations. These are strong indications that fluctuations are strongly dependent on the plasma's density, temperature, presence of large orbit particles, and presence of plasma shear flows, which may influence stability properties of micro-instabilities. Taking

[a)]Electronic mail: calvin.lau@uci.edu
[b)]Electronic mail: zhihongl@uci.edu

inspiration from these observations, we study the stability properties of the microscopic drift-wave instabilities in the FRC plasma, both in the core and in the SOL.

By identifying and studying transport mechanisms, a suitable transport scaling may be found and applied toward predicting confinement performance in larger, hotter, and denser FRC plasmas. To our knowledge, first-principles simulation of turbulent transport in FRC geometry has not been previously carried out. To fill this void in theoretical understanding, and, in support of ongoing experiments at TAE, we extend a mature, well-benchmarked turbulence simulation code, the Gyrokinetic Toroidal Code (GTC),[38,39] to a system with C-2-like geometry and parameters.[35,40,41] The focus of this study is to find and characterize the linear properties of drift-waves in the FRC core and SOL *separately* using gyro-kinetic simulation.

In early work in slab geometry, drift-waves were shown to be always unstable without particular thresholds, thus called "universal instability."[42,43] In the same slab geometry with the addition of finite magnetic shear, however, drift-waves were then found to become completely stabilized.[44–47] The inclusion of electron non-linearity, however, can de-stabilize the drift wave.[48] Investigations of toroidal coupling, in toroidal geometries such as the tokamak, then lead to the de-stabilization of drift-waves yet again.[49–51] In toroidal geometry, the addition of shear flow was then found to be partially stabilizing for the drift-wave instabilities.[52,53] In the last two decades, the paradigm has been dominated by the understanding of zonal flow generation as a non-linear mechanism of regulation for the drift-wave instabilities.[39] With the work of this paper, we address the new aspect of drift-wave stability in the FRC geometry which we are finding quite distinct from those in tokamaks.

In our simulations of the FRC SOL, which has mirror-like and slab-like geometry, the collisionless electrostatic drift-wave in the ion-to-electron-scale is destabilized by the electron temperature gradient due to resonance with locally barely trapped electrons. Collisions suppress this instability, but a collisional drift-wave instability can still exist at realistic pressure gradients.

We find that drift-waves in the FRC core geometry, on the other hand, are robustly stable in simulations (our simulations cover wavelengths up to $k_\zeta \rho_e < 0.3$ so far). We should note here that, unlike tokamak geometry, there is no toroidal coupling which destabilizes the tokamak drift-waves[49–51] in FRC geometry because the FRC lacks the toroidal fields and magnetic shear. Our study in simulations of limiting cases of FRC show this stability to be due to the features of the FRC core: (1) the field-lines of the ideal FRC core geometry are not toroidally coupled, similar to the early slab geometry but with closed field-lines, leading to extremely short connection lengths to shield electronic charge separation; (2) while the curvature of the field-lines is always bad, aligning with the direction of decreasing pressure, but the magnetic field is always increasing radially outward, leading to ∇B drift stabilization; and (3) the high temperature and low magnetic field lead to a large stabilizing finite Larmor radius (FLR) effect.[2,8]

The characteristics of these two regions have been compared to recent TAE experiments[35] and found to be in agreement. In particular, the lack of ion-scale instability in the core is consistent with experimental measurements of a fluctuation spectrum showing a depression in the ion-scale.[35] In addition, linear pressure gradient thresholds for stability found in simulations are consistent with thresholds observed in experiments. The survey of these modes will guide nonlinear and cross-separatrix simulations, as well as simulations including the effects of fast ions and ion cyclotron motion.

The remainder of this paper is organized as follows. Section II briefly details the simulation model which is more explicitly discussed in previous papers.[40,41] Sections III and IV present the results for the core and SOL regions respectively. Section V discusses the interpretation of these results, including comparisons to recent experimental data.[35]

II. SIMULATION MODEL

Electrostatic simulations presented in this paper have been conducted with the Gyrokinetic Toroidal Code (GTC) using gyro-kinetic ions and gyro-kinetic electrons. GTC is a well-benchmarked, first principles code which has been extensively applied to study microturbulence and transport, including ion and electron temperature gradient driven modes,[54] collisionless trapped electron modes,[55] energetic particle transport,[56] Alfvén eigenmodes,[57,58] kink,[59] and tearing modes.[60]

While the FRC core does contain a magnetic null-point, the simulation domains used for this paper do not include the null-point allowing gyro-kinetics to remain valid. This is discussed in Sec. II B and graphically shown in Fig. 1.

Recently, GTC has been extended to study instabilities in the core and scrape-off layer (SOL) regions of the FRC.[40,41] In this work, electrostatic perturbative δf simulations[38,43,61–63] are confined either in the core or SOL region *separately* with no cross-separatrix coupling. The domain is reduced to a toroidal wedge and localized to a single flux surface as described in Subsection II B. The equilibrium parameters of the simulations are detailed in Subsection II A.

A. Equilibrium

Simulations are initialized with a FRC equilibrium which is representative of typical FRC plasmas realized in the C-2 experiment. The equilibrium is calculated using the LR_eqMI code, which is an axisymmetric force balance solver including realistic wall and coil geometry and the possibility of multiple ion species, arbitrary rotation profiles, and arbitrary temperature profiles.[64] These quantities are then transformed[65] from cylindrical coordinates (R, Z, ϕ) to magnetic Boozer coordinates (ψ, θ, ζ) for use in GTC[40] as shown in Fig. 1. The origin of the Boozer coordinate system is located at the magnetic null-point. The magnetic field points in the poloidal direction, $\vec{\theta}$, and the guiding-center drifts are in the toroidal direction, $\vec{\zeta}$, as shown in Fig. 1. Here, the ion diamagnetic direction is positive $(\vec{\zeta})$, and the electron diamagnetic direction is negative $(-\vec{\zeta})$. The major radius $R_0 = 27$ cm is the distance from the machine cylindrical axis (geometry center) to the null-point (magnetic axis) as indicated by the blue dashed line. The minor radius $a = 11$ cm is the distance from the null-point to the separatrix. The separatrix radius $R_s = 38$ cm is the distance from

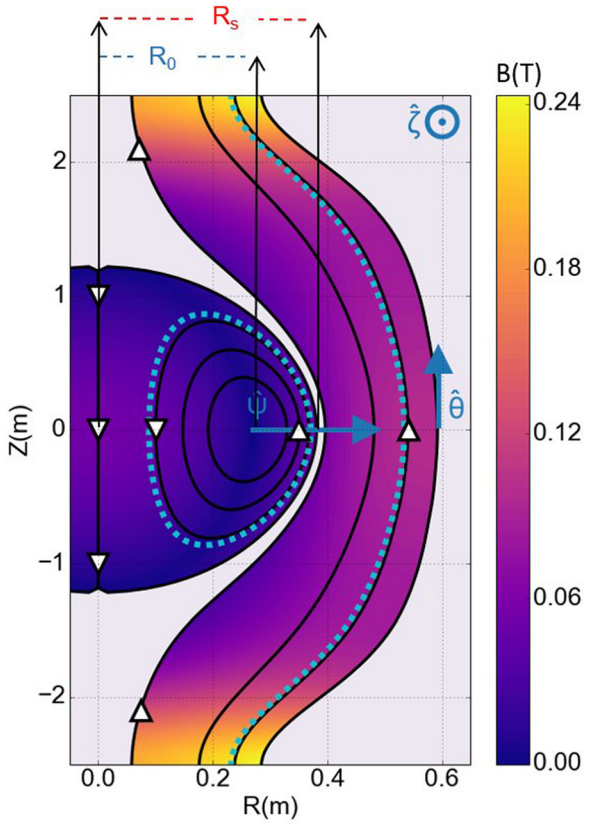

FIG. 1. The field-aligned mesh on a poloidal plane of a typical C-2 FRC discharge is plotted along with the magnitude of the magnetic field represented by color. The flux surfaces used in simulations are represented by dashed cyan lines. Note that the axes are not proportionally scaled. Arrows denote the directions of the magnetic Boozer coordinate system.

the machine cylindrical axis to the separatrix. These are all measured along the mid-plane ($\theta = 0$ or $Z = 0$).

The equilibrium used corresponds to an early time in a C-2 discharge, just after the CTs merge to form a single FRC before a significant fast ion population has built up. At this stage, the size of the plasma is large and diagnostics are more robust. In the simulations, temperature and density gradients are input to drive instabilities in plasma composed of deuterons and electrons. Parameters are chosen to resemble the conditions of recent experiments at TAE[35] and are summarized in Table I. The calculated quantities are the ion gyro-radius $\rho_i = \sqrt{m_i T_i}/(eB)$, electron gyro-radius $\rho_e = \sqrt{m_e T_e}/(eB)$, and ion acoustic speed $C_s = \sqrt{(T_i + T_e)/m_i}$.

TABLE I. Parameters used in simulations of core and SOL.

Quantities	Core	SOL
n_e (cm^{-3})	4.0×10^{13}	2.0×10^{13}
T_e (eV)	80	40
T_i (eV)	400	200
ρ_i (cm)	6.0	2.2
ρ_e (cm)	0.044	0.016
$\frac{R_0}{C_s}$ (μs)	1.8	2.5
ν^*_{e-i}	2.1	5.7
ν^*_{i-i}	0.10	0.27

Temperature and density gradients drive the instabilities. The strengths of these drives are defined by their scale lengths normalized by the machine scale length (where the local minor radius r is the distance measured from the null-point along $\theta = 0$)

$$\kappa_f = \frac{R_0}{L_f} = \frac{R_0}{f}\frac{\partial}{\partial r} f. \tag{1}$$

The drives used are the density gradient $\kappa_n = R_0/L_n$, ion temperature gradient $\kappa_{T_i} = R_0/L_{T_i}$, and electron temperature gradient $\kappa_{T_e} = R_0/L_{T_e}$. In addition, the importance of the drives can be defined by the ratios between the scale lengths of the temperature gradients and the density gradient, $\eta_i = \kappa_{T_i}/\kappa_n$ and $\eta_e = \kappa_{T_e}/\kappa_n$. In most of the simulations presented, the strengths of the three drives are equal, i.e., $\eta_i = \eta_e = \eta = 1$, and the magnitude of the drive strength would then be referred to as $\kappa (= \kappa_n = \kappa_{T_i} = \kappa_{T_e})$.

Simulations were run both with and without collisions based on the Fokker-Planck model[66] to understand the effects of collisions. The effective collisionality is the collisional frequency normalized by the transit frequency and is calculated by $\nu^*_{e-e} = \nu_{e-e}/\omega_{tr,e}$, $\nu^*_{e-i} = \nu_{e-i}/\omega_{tr,e}$, $\nu^*_{i-i} = \nu_{i-i}/\omega_{tr,i}$. The transit frequency of an electron and ion passing along a field-line is $\omega_{tr,e} = V_{th,e}/L$ and $\omega_{tr,i} = V_{th,i}/L$, respectively. Here, $V_{th-i} = \sqrt{T_i/m_i}$ is the ion thermal velocity, and $V_{th-e} = \sqrt{T_e/m_e}$ is the electron thermal velocity. In our simulation domain, the field-line length of the core is $L \approx 3.6$ m, while the field-line length of the SOL is $L \approx 5.0$ m. The effective collisionality is high in both regions for the colder electrons, but low for the hotter ions with a low ion impurity modeled by $Z_{eff} = 1.5$ in both regions.

B. Flux-tube domain

The focus of this study is to characterize the local linear properties of the FRC instabilities in the core and SOL *separately*. The large number of simulations is enabled by the reduction of the simulation domain from a full torus $[0, 2\pi]$ to a partial torus $[0, 2\pi/n]$ where n is the particular toroidal mode number of interest. In these simulations, the toroidal wavelength is assumed to be much shorter than the radial wavelength of the instabilities, i.e., $k_r \ll k_\zeta$.

The radial domain is thus localized to a single flux surface where $R_0 + r = 37$ cm in the core and $R_0 + r = 52$ cm in the scrape-off layer as shown in Fig. 1. These flux surfaces *do not* include the magnetic null-point, allowing the guiding-center approximation to remain valid.[67] The average gyro-kinetic parameter is $\rho_i/L_B \simeq 0.2$ in the core and $\rho_i/L_B \simeq 0.006$ in the SOL which are gyro-kinetically valid (about 1.3% difference between the guiding-center and orbit-averaged positions in case of $\rho_i/L_B \simeq 0.2$ as shown by Brizard[67]).

In this gyro-kinetic simulation,[68] dynamics faster than ion gyro-period are removed while ion and electron finite Larmor radius (FLR) effects are retained through accurate representation of gyro-averaging on particles via direct calculations of Bessel functions for the scattering of charge onto the grid and in the gathering of fields onto the charge.

Due to the neglect of radial gyro-averaging, the growth-rate of instability is expected to be higher when compared to non-local simulations. Previous work by Naitou *et al.*[5] with fully kinetic particle dynamics also supports the expectation of strongly stabilizing FLR effects.

III. STABLE DRIFT-WAVES IN THE FRC CORE

Within gyro-kinetically valid regimes

$$\frac{\omega}{\Omega_i} \sim \frac{\rho_i}{L_B} \sim \frac{e\phi}{T} < 1, \quad \frac{k_\parallel}{k_\perp} \ll 1, \tag{2}$$

(where ρ_i is the ion gyro-radius, $L_B = \frac{1}{B}\frac{\partial B}{\partial r}$ is the magnetic field scale length, and ϕ is the perturbed electrostatic potential) the electrostatic drift-wave is found to be stable in the FRC core when driven by pressure gradients relevant to the C-2 advanced beam driven FRC experiment. Simulations with equal temperature and density gradients ($\eta_i = \eta_e = \eta = 1$) and with drive strengths up to $\frac{R_0}{L_n} = \kappa_n < 5$ were performed. Toroidal wavelengths were scanned from ion scale to electron scale up to $k_\zeta \rho_e < 0.3$. From these GTC simulations, the FRC core is found to be stable within this regime.

A. Mechanisms for core stability

To understand this surprising stability, further simulations based on limiting cases were studied.

From magnetohydrodynamics, the radially increasing quantity $\oint \frac{dl}{B}$ suggests the existence of a flute instability in the core. An instability can be found by suppressing particle motion in the simulation by evolving only particle weight (δf) and holding particle positions and velocities fixed (i.e., initial phase space coordinates of particles are fixed). This indicates the importance of electron kinetics for stability. Work based on this instability also finds both the finite Larmor radius[2] (FLR) and the ∇B effects to be additional stabilization effects as expected. Similar simulations turning on and off FLR and ∇B effects were also performed in the SOL and are detailed in Sec. IV. Simulations also find that only the electron kinetic effects need to be suppressed for the core to exhibit this instability.

In simulations of purely $k_\parallel = 0$ but with the evolution of both particle weight and phase space positions, in the limit of far-from-experimental conditions (for example, temperature 100× lower), stability persists when FLR effects are kept; however, when FLR effects are turned off at these limiting case conditions, the $k_\parallel = 0$ mode can become unstable.

Additional limiting conditions further show the importance of electron kinetic effects. In the limit of artificially heavy electrons ($m_e/m_p > 0.25$–0.5), an unstable mode peaking in the outer mid-plane can exist. In the limit of artificially elongated geometry approaching a theta-pinch-like geometry ($Z_{lim}/Z_0 < 5$–7, where Z_{lim} is the artificially elongated length and Z_0 is the original C-2-like length), a similar unstable mode can also form in the outer mid-plane. These limiting cases suggest the electron kinetic effects, and, especially, the short electron transit time (as slower velocities or longer travel length contribute to) to be important FRC features which contribute to the core stability.

The broad stability of the core within the C-2-like parameters may provide the basis for understanding some of the experimentally observed phenomena. Experiments observe robust fluctuations in the SOL and fluctuations of an order of magnitude smaller in the core.[35] Furthermore, in the same experiments, the core spectrum exhibits a depression in the ion range ($k_\zeta \rho_s < 15$) unlike the SOL spectrum.

Because our linear, local simulations do not include the stabilizing influences of fast ions and non-local effects which exist in the experiments, instabilities should be enhanced within these simulations. However, quite the opposite, the results of the simulations show the core stability to be extremely robust.

It should be noted that one element missing from these simulations may explain fluctuations in the core: the coupling of the SOL and core. Cross-separatrix coupling between the two regions may introduce fluctuations originating from the SOL (detailed in Sec. IV) into the core which, by itself, is found to be inherently stable.

IV. DRIFT-WAVE INSTABILITIES IN THE SCRAPE-OFF LAYER (SOL)

A. Collisionless $\eta = 1$ instability

GTC simulations were also performed for the SOL, using C-2-like parameters detailed in Table I with $\eta = 1$. Relative to the core, the temperatures and densities of both species are lowered by a factor of 2 while the magnitude of the background magnetic field is roughly stronger by a factor of 2. Under these conditions, simulations show the existence of unstable modes ranging from ion-scale to electron-scale wavelengths. This is consistent with SOL experimental measurements of density fluctuations which exhibit an exponential spectrum ranging from the ion-scale to electron-scale.[35]

Figure 2 shows the instability frequency (ω_r) and growth-rate (γ) over a range of $k_\zeta \rho_s$ for various drive strengths. ω_r is in the electron diamagnetic direction and the electron curvature drift direction, but opposite to the electron ∇B drift direction. As $k_\zeta \rho_s$ increases, the magnitude of ω_r

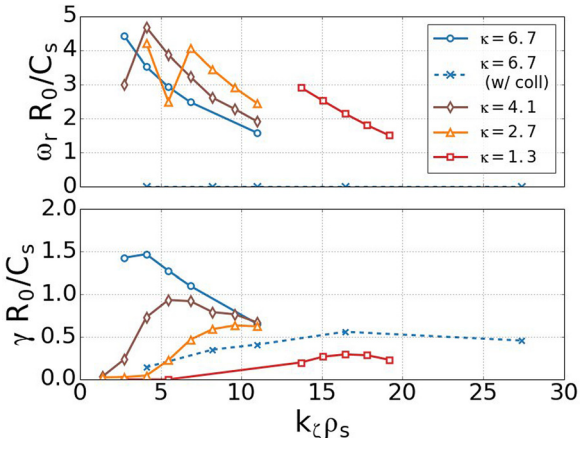

FIG. 2. Real frequency (ω_r) and growth-rate (γ) for different drive strengths (κ) of the collisionless SOL instability for $\eta = 1$ are shown as solid lines. For comparison, the dispersion of the collisional SOL instability for $\eta = 1$ is shown as the dashed line. As the drive decreases, the instability shifts toward the shorter wavelength (k_ζ).

decreases until a jump up to a similar frequency which trends downward again. This jump is associated with a change in the poloidal mode structure from odd parity about the mid-plane to even parity.

A stability threshold is found at drive strength around $\kappa_{sim} \approx 3$–5 for longer wavelengths as seen in Fig. 3, which is comparable to $\kappa_{exp} \approx 3.9$ as measured in experiments. Shorter wavelengths are found to have lower stability thresholds.

As seen in the mid-panel of Fig. 4, the mode structure in the SOL spans the field-line length is dominated by poloidal mode numbers $m = 1$ with smaller components of $m = 0$ and $m = 2$ (where the poloidal direction is the horizontal axis). The central location of the mode can be explained by the effects of gyro-averaging and by the behavior of the resonant particles. As seen in Fig. 1, k_ζ is lower at the mid-plane ($Z \sim 0$) and higher at the axial ends ($Z \sim \pm 2$) by more than a factor of two, leading to a weaker gyro-averaging effect in the central location. The dominant particle resonance is due to *barely trapped electrons* in the central location, as seen in the figure-8 structure in the $v_\parallel - \theta$ phase-space plot in Fig. 4 (detailed in Sec. IV B).

B. Particle resonances

The square of the perturbed distribution functions δf^2 is plotted in the plane of energy (E/T) vs pitch angle ($\mu B_0/E$) for both species in Fig. 5 for the $k_\zeta \rho_s = 4.1$ ($n = 75$, $\eta = 1$, $\kappa = 6.7$). For this instability, electron resonance is more important than ion resonance ($\delta f_e^2 > \delta f_i^2$). The resonant ion motion is the drift due to ∇B and curvature, as shown by the curves in the upper panel of Fig. 5. More importantly, the resonant electron motion which drives this instability is shown to be the bounce motion of *barely trapped electrons*, as shown in the lower panel of Fig. 5.

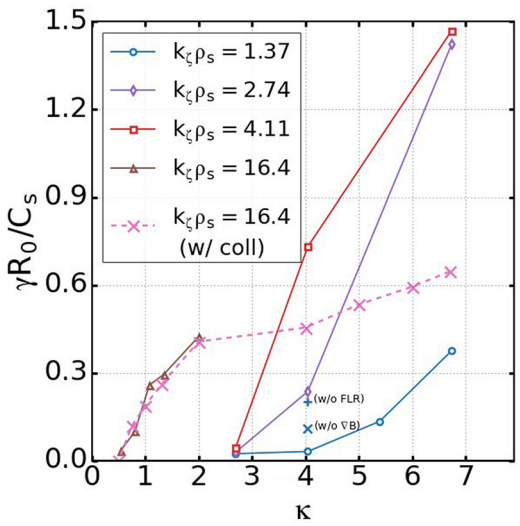

FIG. 3. Growth-rates (γ) vs drives (κ) for unstable collisionless SOL modes for $\eta = 1$ at various length-scales are plotted as solid lines. The unstable collisional $k_\zeta \rho_s = 16.4$ mode for $\eta = 1$ is also plotted as the dashed line. The threshold is found to be lower for shorter wavelengths.[35] The growth-rates for $k_\zeta \rho_s = 1.37$ (blue) without FLR effects (+) and without ∇B effects (x) are also plotted for comparison.

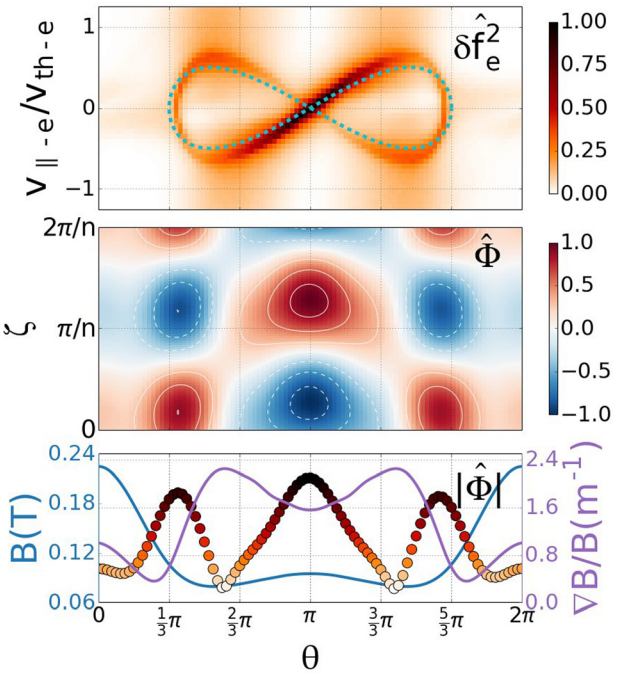

FIG. 4. The top panel shows the $v_\parallel - \theta$ phase-space of the electrons with the color representing δf_e^2. The middle panel shows the electrostatic potential in the $\zeta - \theta$ plane for the case of $k_\zeta \rho_s = 4.1$ ($n = 75$, $\eta = 1$, and $\kappa = 6.7$). The bottom panel shows the potential along the poloidal direction for $\zeta = 0$. In addition, the magnitude and the radial gradient of the magnetic field are shown as the blue and purple curves corresponding to the left and right axes, respectively.

The electrons can be separated into three groups: locally trapped electrons, globally trapped electrons, and passing electrons. In the SOL, the geometry is such that there are two small magnetic wells and an overall large magnetic well as seen in the blue curve of the bottom panel of Fig. 4. *Locally trapped electrons* are bound within the two smaller magnetic wells. *Globally trapped electrons* are bound within the overall larger magnetic well. *Passing electrons* are able to freely stream through the magnetic well in the periodic domain. The boundaries of these trapped-passing regimes are denoted by the arrows in Fig. 5. From the perturbed distributions of the electrons in Fig. 5, it can be clearly seen that the mode frequency is aligned with the bounce frequency of the barely locally trapped electrons at $\mu B_0/E = 1$. This resonant motion can also been seen when the perturbed electron distribution function is plotted in phase space ($v_\parallel$ vs θ) as in the top panel of Fig. 4. The figure-8 shape highlights the motion of the barely trapped electrons moving back and forth within the magnetic well.

Further evidence of the importance of this bounce motion of the electrons in driving this instability is seen from the case of purely density gradient driven instability ($\eta = 0$) and the case of ion-temperature and density gradient driven instability ($\eta_i = 1$) (detailed in Sec. IV C).

C. Stabilizing mechanisms

As in the core, the stabilizing influences of the finite Larmor radius (FLR) and magnetic well (negative ∇B) are explored in the SOL by turning on and off these effects in

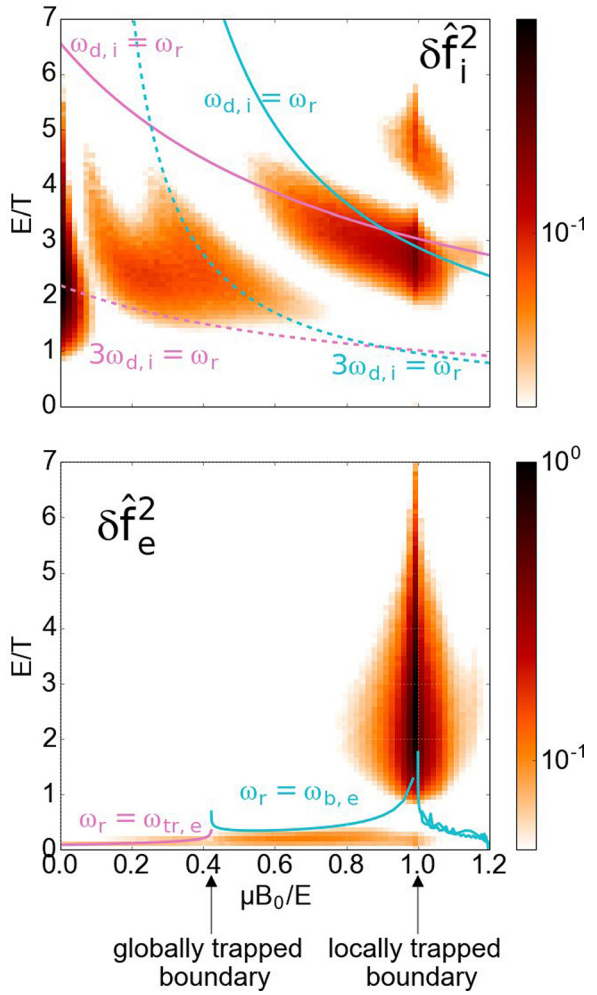

FIG. 5. δf^2 (normalized by the maximum δf_e^2) is plotted for the ions (upper panel) and electrons (lower panel) with respect to energy and pitch angle. For ions, curves represent the ion drift frequency; pink (cyan) corresponds to values calculated at $\theta = \pi$ ($\theta = \pi/3$). For electrons, the pink (cyan) corresponds to the electron transit frequency (electron bounce frequency).

simulations. This is shown for the $k_\zeta \rho_s = 1.37$ case for $\kappa \sim 4$ in Fig. 3. Like the core, it is found that the FLR effect is more strongly stabilizing than the ∇B effect when the drive is strong. However, when the drive is marginal, as might be expected from self-organization of the plasma, both are important in the complete suppression of instability.

In the experiments, the temperature gradients can actually be stronger than the density gradients. In the simulations presented in Sec. IV A, the gradients of the density, ion temperature, and electron temperature are equal. In order to better understand the drive of the instability for $\eta = 1$, simulations of the $k_\zeta \rho_s = 4.1$ instability were repeated with the density gradient unchanged at $\kappa_n = 6.7$ while *separately* varying the ion temperature gradient κ_{T_i} and electron temperature gradient κ_{T_e}. As shown in Fig. 6, the electron temperature gradient is destabilizing while the ion temperature gradient is stabilizing. In addition, this instability exists even when there is only a density gradient ($\eta_e = \eta_i = 0$, $\kappa_n \neq 0$).

These results can be understood by looking at the electron perturbed distribution functions. In the $\eta = 0$ case as shown in the top panel of Fig. 7, the resonant electrons are at

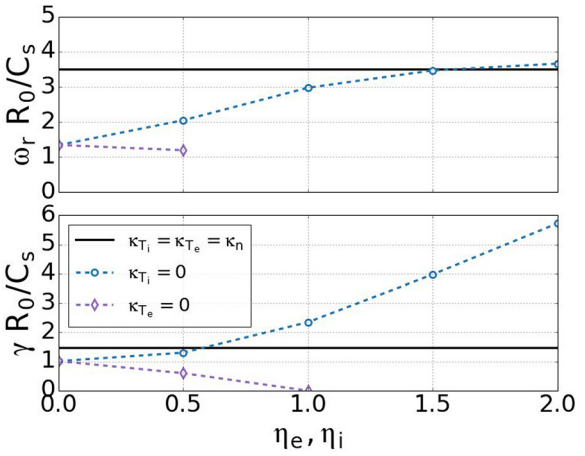

FIG. 6. Dispersion relation with respect to η_e (η_i) is plotted as the blue (purple) dashed lines. The frequency and growth-rate for the $\eta = 1$ (black) case is plotted as the solid line for comparison. The density gradient drive κ_n is kept constant while κ_{T_e} (κ_{T_i}) is varied for the η_e (η_i) scan. Note that the mode is unstable even with only κ_n.

lower energy in contrast to the $\eta = 1$ case. The electron resonance is also no longer dominated by the locally barely trapped electrons but still by trapped electrons. In the $\eta_e = 1$, $\eta_i = 0$ case, the frequency is comparable to the $\eta = 1$ case but

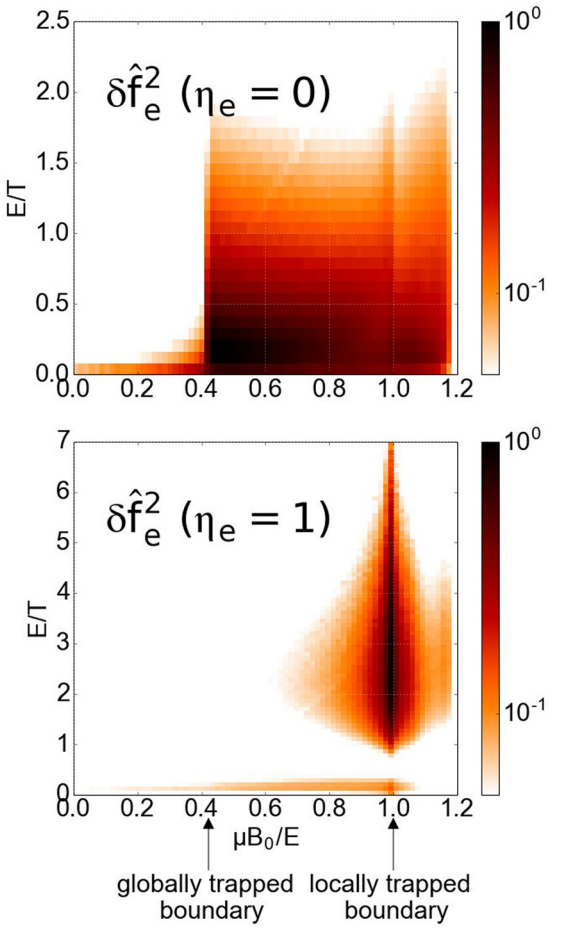

FIG. 7. The δf_e^2 (normalized by the maximum δf_e^2) is plotted for $\eta_e = 0$ and $\eta_e = 1$ with respect to energy and pitch angle. When the electron temperature gradient (κ_{T_e}) is decreased ($\eta_e = 1 \rightarrow \eta_e = 0$), the electron resonance shifts from locally trapped to globally trapped.

with even faster growth. The resonant ions are at lower energy while the resonant electrons are, as in the $\eta = 1$ case, the high energy locally barely trapped electrons, as seen in the bottom panel of Fig. 7. From the comparison of the three cases, it is clear that the motion of the locally barely trapped electrons is the resonance that drives the collisionless SOL instability.

D. Collisional effects

Using the Fokker-Planck model, the SOL instability for $\eta = 1$ was simulated with pitch-angle scattering through electron-ion collisions over a range of collisionality, from collisionless to the collision frequency defined for $Z_{eff} = 1.5$ using equilibrium densities and temperatures detailed in Table I. With collisions, both frequency and growth-rate decrease, but as the collisionality is lowered, the collisionless frequency and growth-rate are recovered. While collisions are strongly stabilizing in the long wavelength case, there is negligible effect to the mode structure, which is strongly dominated by the $m = 0$ and $m = 1$ harmonics.

The effect of collisions on this instability can be understood from the locally trapped electron resonance. Pitch-angle scattering frequently moves electrons in and out of that particular energy-pitch position, essentially removing the drive of this instability. However, as seen in Figs. 2 and 3, there is still a significant instability which can exist at shorter wavelengths even when the collisionless mode is suppressed by collisions.

V. DISCUSSION

Local gyrokinetic simulations have been used to investigate electrostatic pressure gradient-driven drift-waves in the FRC. While the FRC core was expected to be less unstable[1] due to the large ion gyro-radius, simulations found drift-waves in the core to be completely stable with C-2-like parameters for pressure gradient drives up to $\rho_i/L_P \leq \mathcal{O}(1)$ with equal temperature and density gradients ($\eta = 1$) for ion-to-electron scale wavelengths ($k_\zeta \rho_e < 0.3$). Our studies of limiting cases in the FRC strongly suggest that this stability is due to the short electron connection length with further stabilizing contribution from FLR[8] and ∇B effects. Only when the FRC geometry is artificially elongated from the typical C-2-like FRC toward the field-reversed theta pinch (by Z_{lim}/Z_0 exceeding 5–7) does the known drift-wave instability appear, consistent with the importance of electron parallel dynamics. It should also be noted that the electron connection length along the field-lines in the FRC core is much shorter than those such as in tokamaks.

In the SOL, a pressure gradient driven mode with wavelengths ranging from ion-scale to electron-scale has been found. This collisionless instability is driven by magnetically trapped electrons. The unstable mode peaks are correlated with the regions with weakest magnetic fields, strongest curvature, and local minima of ∇B. Collisions suppress this instability but allow a different lower frequency collisional instability at shorter wavelengths.

In experiments conducted by Schmitz *et al.*,[35] density fluctuations measured in the core display a "depressed" wavenumber spectrum in which fluctuation amplitudes are low at ion-scale wavelengths but peak at electron-scale wavelengths (in the range around $k_\zeta \rho_e \approx 0.15$–$0.45$). The fluctuations measured in the SOL have a more typical wavenumber spectrum with higher amplitudes at ion-scale and exponentially decreasing amplitudes toward shorter wavelengths. The stability exhibited in the simulations of the core is consistent with the experimental core fluctuation spectrum; however, simulations using Vlasov ions are necessary to explore the possibility of higher frequency instabilities. The ion-to-electron-scale nature of the instability of the SOL displayed in simulations is consistent with the experimentally measured SOL fluctuation spectrum. In addition, experimental data show the existence of fluctuation thresholds[35] at normalized drive strengths of $\kappa_{exp} \approx 3.9$. In simulations, collisionless linear thresholds are found at $\kappa_{sim} \approx 3$–5 in the SOL for the longer wavelength modes.

Based on the fastest growth-rates of the collisionless SOL instability driven by the largest and smallest simulated drive strengths $\kappa \approx 8.1$–1.3, the characteristic growth times are $\gamma \approx 1.75 \sim 0.25 C_s/R_0 \rightarrow \tau_{SOL} = 1.4$–$10$ μs. The fastest growing collisional SOL mode, driven by $\kappa = 6.7$, has a comparable growth time of $\gamma \approx 0.65 C_s/R_0 \rightarrow \tau_{SOL} = 3.9$ μs. In the C-2 experiments, the FRC plasma lifetimes are on the order of milliseconds, and so both the collisionless and collisional SOL modes have enough time to grow to a substantial amplitude to explain the fluctuation spectrum observed.

In experimental measurements of density fluctuations,[35] the FRC core and SOL show distinct behaviors. The SOL displays strong density fluctuations which follow an exponential scaling while the quiescent core density fluctuations are lower in amplitude by an order of magnitude. In agreement with these experimental results, our simulations find drift-waves to be robustly stable in the core and unstable in the SOL.

The surprising stability of electrostatic drift-waves in the core requires further studies to isolate the origin of the fluctuations observed in experiments. Higher frequency instabilities may exist in the core, but the origin of the fluctuations may also lie in the interaction between the SOL and core. Future work will focus on the physics of cross-separatrix interactions and the possible propagation of fluctuations from SOL to core.

ACKNOWLEDGMENTS

The authors would like to thank Sean Dettrick and the TAE team at Tri Alpha Energy, Inc., for equilibrium data as well as the ongoing insights and collaboration in the development of these simulations. This work was carried out at University of California, Irvine, with the support of the Norman Rostoker Fellowship (Grant No. TAE-200441) and by the DOE SciDAC GSEP center. Simulations used the resources of the Oak Ridge Leadership Computing Facility at the Oak Ridge National Laboratory (DOE Contract No. DE-AC05-00OR22725) and the National Energy Research Scientific Computing Center (DOE Contract No. DE-AC02-05CH11231).

[1]N. Rostoker, F. Wessel, H. Rahman, B. C. Maglich, B. Spivey, and A. Fisher, "Magnetic fusion with high energy self-colliding ion beams," Phys. Rev. Lett.. **70**, 1818–1821 (1993).

[2]N. Rostoker, "Closing remarks," in *Physics of High Energy Particles in Toroidal Systems*, edited by T. Tajima and M. Okamoto (AIP Publishing, 1994), Vol. 1.
[3]M. W. Binderbauer and N. Rostoker, "Turbulent transport in magnetic confinement: How to avoid it," J. Plasma Phys. **56**, 451–465 (1996).
[4]D. C. Barnes, J. L. Schwarzmeier, H. R. Lewis, and C. E. Seyler, "Kinetic tilting stability of field-reversed configurations," Phys. Fluids **29**(8), 2616–2629 (1986).
[5]H. Naitou, T. Kamimura, and J. M. Dawson, "Kinetic effects on the convective plasma diffusion and the heat transport," J. Phys. Soc. Jpn. **46**(1), 258–265 (1979).
[6]R. Horiuchi and T. Sato, "Full magnetohydrodynamic simulation of the tilting instability in a field reversed configuration," Phys. Fluids B **1**(3), 581–590 (1989).
[7]W. W. Heidbrink and G. J. Sadler, "The behaviour of fast ions in tokamak experiments," Nucl. Fusion **34**(4), 535 (1994).
[8]M. Rosenbluth, N. Krall, and N. Rostoker, "Finite Larmour radius stabilization of "weakly" unstable confined plasmas," Nucl. Fusion Supp. **1**, 143 (1962), available at https://www.osti.gov/scitech/biblio/4808729.
[9]M. W. Binderbauer, H. Y. Guo, M. Tuszewski, S. Putvinski, L. Sevier, D. Barnes, N. Rostoker, M. G. Anderson, R. Andow, L. Bonelli *et al.*, "Dynamic formation of a hot field reversed configuration with improved confinement by supersonic merging of two colliding high-β compact toroids," Phys. Rev. Lett. **105**, 045003 (2010).
[10]H. Guo, M. Binderbauer, T. Tajima, R. Milroy, L. Steinhauer, X. Yang, E. Garate, H. Gota, S. Korepanov, A. Necas *et al.*, "Achieving a long-lived high-beta plasma state by energetic beam injection," Nat. Commun. **6**, 6897 (2015).
[11]M. Tuszewski, A. Smirnov, M. C. Thompson, T. Akhmetov, A. Ivanov, R. Voskoboynikov, D. C. Barnes, M. W. Binderbauer, R. Brown, D. Q. Bui *et al.*, "A new high performance field reversed configuration operating regime in the c-2 device," Phys. Plasmas **19**(5), 056108 (2012).
[12]M. W. Binderbauer, T. Tajima, L. C. Steinhauer, E. Garate, M. Tuszewski, L. Schmitz, H. Y. Guo, A. Smirnov, H. Gota, D. Barnes *et al.*, "A high performance field-reversed configuration," Phys. Plasmas **22**(5), 056110 (2015).
[13]S. Hamasaki and D. Book, "Numerical simulation of the anomalous transport process in radially compressed reversed-field configurations," Nucl. Fusion **20**(3), 289 (1980).
[14]M. Tuszewski and R. K. Linford, "Particle transport in field-reversed configurations," Phys. Fluids **25**(5), 765–774 (1982).
[15]A. L. Hoffman, R. D. Milroy, and L. C. Steinhauer, "Poloidal flux loss in a field-reversed theta pinch," Appl. Phys. Lett. **41**, 31–33 (1982).
[16]A. W. Carlson, "A search for lower-hybrid-drift fluctuations in a field-reversed configuration using CO_2 heterodyne scattering," Phys. Fluids **30**(5), 1497–1509 (1987).
[17]D. Winske and P. C. Liewer, "Particle simulation studies of the lower hybrid drift instability," Phys. Fluids **21**(6), 1017–1025 (1978).
[18]J. U. Brackbill, D. W. Forslund, K. B. Quest, and D. Winske, "Nonlinear evolution of the lower-hybrid drift instability," Phys. Fluids **27**(11), 2682–2693 (1984).
[19]N. T. Gladd, A. G. Sgro, and D. W. Hewett, "Microstability properties of the sheath region of a field-reversed configuration," Phys. Fluids **28**(7), 2222–2234 (1985).
[20]N. T. Gladd, J. F. Drake, C. L. Chang, and C. S. Liu, "Electron temperature gradient driven microtearing mode," Phys. Fluids **23**(6), 1182–1192 (1980).
[21]R. K. Linford, "Los Alamos compact toroid, fast liner, and high-density z-pinch programs," in *Unconventional Approaches to Fusion*, edited by B. Brunelli and G. G. Leotta (Plenum Press, New York and London, 1982), Vol. 13, p. 463.
[22]A. L. Hoffman and R. D. Milroy, "Particle lifetime scaling in field-reversed configurations based on lower-hybrid-drift resistivity," Phys. Fluids **26**(11), 3170–3172 (1983).
[23]S. P. Auerbach and W. C. Condit, "Classical diffusion in a field-reversed mirror," Nucl. Fusion **21**(8), 927 (1981).
[24]K. Nguyen and T. Kammash, "Classical transport coefficients in a field-reversed configuration," Plasma Phys.. **24**(2), 177 (1982).
[25]R. A. Clemente and C. E. Grillo, "Internal tilting and classical transport for field-reversed configurations based on the Maschke-Hernegger solution," Phys. Fluids **27**(3), 658–660 (1984).
[26]R. A. Clemente and E. M. Freire, "Classical particle-diffusion time for analytical compact tori equilibria," Plasma Phys. Controlled Fusion **28**(7), 951 (1986).
[27]Y. Aso, S. Himeno, and K. Hirano, "Experimental studies on energy transport in a reversed-field theta pinch," Nucl. Fusion **23**(6), 751 (1983).
[28]D. J. Rej and M. Tuszewski, "A zero-dimensional transport model for field-reversed configurations," Phys. Fluids **27**(6), 1514–1520 (1984).
[29]S. Hamada, "A model of equilibrium transport and evolution of field reversed configurations," Nucl. Fusion **26**(6), 729 (1986).
[30]D. C. Quimby, A. L. Hoffman, and G. C. Vlases, "Linus cycle calculations including plasma transport and resistive flux loss," Nucl. Fusion **21**(5), 553 (1981).
[31]E. J. Caramana, "The long-time evolution approximation for a quasi-one-dimensional plasma system," Phys. Fluids **28**(12), 3557–3566 (1985).
[32]K. A. Werley, "One-and-a-quarter-dimensional transport modeling of the field-reversed configuration," Phys. Fluids **30**(7), 2129–2138 (1987).
[33]D. E. Shumaker, "Transport simulation of a field-reversed configuration plasma," Fusion Sci. Technol. **13**, 555 (1988).
[34]M. Binderbauer, T. Tajima, M. Tuszewski, L. Schmitz, A. Smirnov, H. Gota, E. Garate, D. Barnes, B. Deng, E. Trask *et al.*, "Recent breakthroughs on c-2u: Norman's legacy," in *The Physics of Plasma-Driven Accelerators and Accelerator-Driven Fusion: The Proceedings of Norman Rostoker Memorial Symposium*, edited by T. Tajima and M. Binderbauer (AIP Publishing, Melville, NY, 2016), p. 030003.
[35]L. Schmitz, D. Fulton, E. Ruskov, C. Lau, B. Deng, T. Tajima, M. Binderbauer, I. Holod, Z. Lin, H. Gota *et al.*, "Suppressed ion-scale turbulence in a hot high-β plasma," Nat. Commun. **7**, 13860 (2016).
[36]S. Gupta, D. Barnes, S. Dettrick, E. Trask, M. Tuszewski, B. Deng, H. Gota, D. Gupta, K. Hubbard, S. Korepanov *et al.*, "Transport studies in high-performance field reversed configuration plasmas," Phys. Plasmas **23**(5), 052307 (2016).
[37]M. Y. Hsiao, K. A. Werley, and K. M. Ling, "CFRX, a one-and-a-quarter-dimensional transport code for field-reversed configuration studies," Comput. Phys. Commun. **54**(2), 329–352 (1989).
[38]I. Holod, W. L. Zhang, Y. Xiao, and Z. Lin, "Electromagnetic formulation of global gyrokinetic particle simulation in toroidal geometry," Phys. Plasmas **16**(12), 122307 (2009).
[39]Z. Lin, T. S. Hahm, W. W. Lee, W. M. Tang, and R. B. White, "Turbulent transport reduction by zonal flows: Massively parallel simulations," Science **281**, 1835 (1998).
[40]D. Fulton, C. Lau, I. Holod, Z. Lin, and S. Dettrick, "Gyrokinetic particle simulation of a field reversed configuration," Phys. Plasmas **23**(1), 012509 (2016).
[41]D. Fulton, C. Lau, L. Schmitz, I. Holod, Z. Lin, T. Tajima, M. Binderbauer, and TAE Team, "Gyrokinetic simulation of driftwave instability in field-reversed configuration," Phys. Plasmas **23**, 056111 (2016).
[42]A. B. Mikhailovskii, "Weakly inhomogeneous collisionless plasma," in *The Theory of Plasma Instabilities: Instabilities of an Inhomogeneous Plasma* (Springer US, New York, 1974), Vol. 2, p. 49.
[43]T. Tajima, "Guiding-center method," in *Computational Plasma Physics: With Applications to Fusion and Astrophysics* (Addison-Wesley, Redwood City, CA, 1989), Vol. 1, p. 189.
[44]L. Pearlstein and H. Berk, "Universal eigenmode in a strongly sheared magnetic field," Phys. Rev. Lett. **23**(5), 220 (1969).
[45]D. W. Ross and S. M. Mahajan, "Are drift-wave eigenmodes unstable?," Phys. Rev. Lett. **40**(5), 324 (1978).
[46]K. Tsang, J. Whitson, J. Callen, P. Catto, and J. Smith, "Drift Alfven waves in tokamaks," Phys. Rev. Lett. **41**(8), 557 (1978).
[47]R. Sydora, J. Leboeuf, and T. Tajima, "Particle simulation of drift waves in a sheared magnetic field," Phys. Fluids **28**(2), 528–537 (1985).
[48]S. Hirshman and K. Molvig, "Turbulent destabilization and saturation of the universal drift mode in a sheared magnetic field," Phys. Rev. Lett. **42**(10), 648 (1979).
[49]C. Cheng and L. Chen, "Unstable universal drift eigenmodes in toroidal plasmas," Phys. Fluids **23**(9), 1770–1773 (1980).
[50]L. Chen, M. Chance, and C. Cheng, "Absolute dissipative drift-wave instabilities in tokamaks," Nucl. Fusion **20**(7), 901 (1980).
[51]J. Connor, R. Hastie, and J. Taylor, "Stability of general plasma equilibria. III," Plasma Phys. **22**(7), 757 (1980).
[52]M. LeBrun, T. Tajima, M. Gray, G. Furnish, and W. Horton, "Toroidal effects on drift wave turbulence," Phys. Fluids B **5**(3), 752–773 (1993).
[53]Y. Kishimoto, T. Tajima, W. Horton, M. LeBrun, and J. Kim, "Theory of self-organized critical transport in tokamak plasmas," Phys. Plasmas **3**(4), 1289–1307 (1996).
[54]Z. Lin, I. Holod, L. Chen, P. H. Diamond, T. S. Hahm, and S. Ethier, "Wave-particle decorrelation and transport of anisotropic turbulence in collisionless plasmas," Phys. Rev. Lett. **99**(26), 265003 (2007).

[55]Y. Xiao and Z. Lin, "Turbulent transport of trapped-electron modes in collisionless plasmas," Phys. Rev. Lett. **103**(8), 085004 (2009).
[56]W. Zhang, Z. Lin, and L. Chen, "Transport of energetic particles by microturbulence in magnetized plasmas," Phys. Rev. Lett. **101**(9), 095001 (2008).
[57]H. S. Zhang, Z. Lin, and I. Holod, "Nonlinear frequency oscillation of Alfven eigenmodes in fusion plasmas," Phys. Rev. Lett. **109**(2), 025001 (2012).
[58]Z. Wang, Z. Lin, I. Holod, W. W. Heidbrink, B. Tobias, M. Van Zeeland, and M. E. Austin, "Radial localization of toroidicity-induced Alfven eigenmodes," Phys. Rev. Lett. **111**(14), 145003 (2013).
[59]J. McClenaghan, Z. Lin, I. Holod, W. Deng, and Z. Wang, "Verification of gyrokinetic particle simulation of current-driven instability in fusion plasmas. I. Internal kink mode," Phys. Plasmas **21**(12), 122519 (2014).
[60]D. Liu, W. Zhang, J. McClenaghan, J. Wang, and Z. Lin, "Verification of gyrokinetic particle simulation of current-driven instability in fusion plasmas. II. Resistive tearing mode," Phys. Plasmas **21**(12), 122520 (2014).
[61]A. Dimits and W. W. Lee, "Partially linearized algorithms in gyrokinetic particle simulation," J. Comput. Phys. **107**(2), 309–323 (1993).
[62]S. E. Parker and W. W. Lee, "A fully nonlinear characteristic method for gyrokinetic simulation," Phys. Fluids B: Plasma Phys. **5**(1), 77–86 (1993).
[63]Z. Lin, Y. Nishimura, Y. Xiao, I. Holod, W. L. Zhang, and L. Chen, "Global gyrokinetic particle simulations with kinetic electrons," Plasma Phys. Controlled Fusion **49**, B163 (2007).
[64]L. Galeotti, D. C. Barnes, F. Ceccherini, and F. Pegoraro, "Plasma equilibria with multiple ion species: Equations and algorithm," Phys. Plasmas **18**(8), 082509 (2011).
[65]W. D. D'haeseleer, W. N. G. Hitchon, J. D. Callen, and J. L. Shohet, "The Clebsch-type coordinate systems," in *Flux Coordinates and Magnetic Field Structure: A Guide to a Fundamental Tool of Plasma Theory*, edited by R. Glowinski, M. Holt, P. Hut, H. B. Keller, J. Killeen, S. A. Orszag, and V. V. Rusanov (Springer-Verlag, Berlin, Germany, 1991).
[66]Z. Lin, W. M. Tang, and W. W. Lee, "Gyrokinetic particle simulation of neoclassical transport," Phys. Plasmas **2**(8), 2975–2988 (1995).
[67]A. J. Brizard, "On the validity of the guiding-center approximation in the presence of strong magnetic gradients," Phys. Plasmas **24**(4), 042115 (2017).
[68]W. W. Lee, "Gyrokinetic approach in particle simulation," Phys. Fluids **26**(2), 556–562 (1983).